GA–A23950

# THE USE OF 1 MW, 110 GHz 10 s GYROTRON SYSTEMS ON THE DIII–D TOKAMAK

by

R. W. CALLIS, W.P. CARY, R. ELLIS, I. GORELOV,
J. HOSEA, J. LOHR, R.I. PINSKER, D. PONCE,
and R. PRATER

APRIL 2002

GA–A23950

# THE USE OF 1 MW, 110 GHz 10 s GYROTRON SYSTEMS ON THE DIII–D TOKAMAK

by

R. W. CALLIS, W.P. CARY, R. ELLIS,[1] I. GORELOV, J. HOSEA,[1] J. LOHR, R.I. PINSKER, D. PONCE, and R. PRATER

This is a preprint of a paper presented at the Third IAEA Technical Committee Meeting on Steady-State Operation of Magnetic Fusion Devices, May 2–3, 2002, Arles, France, and published in the *Proceedings* (on CD-ROM only).

Work supported by
U.S. Department of Energy under Contracts
DE-FG03-99ER54463 and DE-AC02-76CH03073

[1]Princeton Plasma Physics Laboratory

GENERAL ATOMICS PROJECT 30033
APRIL 2002

# The Use of 1 MW, 110 GHz, 10 s Gyrotron Systems on the DIII–D Tokamak

R.W. Callis,[1] W.P. Cary,[1] R. Ellis,[2] I. Gorelov,[1] H.J. Grunloh,[1] J. Hosea,[2]
John Lohr,[1] R.I. Pinsker,[1] D. Ponce,[1] and R. Prater[1]

[1]*General Atomics, P.O. Box 85608, San Diego, California 92186-5608, USA*
[2]*Princeton Plasma Physics Laboratory, P.O. Box 451, Princeton, NJ 08543-0451, USA*

## Abstract

Advances in gyrotron technology are resulting in new capabilities and scientific results on magnetic confinement devices for fusion research worldwide. This has led to successful experiments on electron cyclotron heating, electron cyclotron current drive, non-inductive tokamak operation, tokamak energy transport, suppression of instabilities and advanced profile control leading to enhanced performance. Three 110 GHz gyrotrons with nominal output power of 1 MW each have been installed and are operational on the DIII–D tokamak. All three gyrotrons were built by Communications and Power Industries* (CPI). The CPI gyrotrons utilize a single disc CVD (chemical-vapor-deposition) diamond window that employs water cooling around the edge of the disc. Calculation predict that the CVD diamond window should be capable of full 1 MW cw operation, which is supported by IR camera measurements that show the window reaching equilibrium after 2.5 s. All gyrotrons are connected to the tokamak by low-loss-windowless evacuated transmission line using circular corrugated waveguide for propagation in the $HE_{11}$ mode. Each waveguide system incorporates a two-mirror launcher, which can steer the rf beam poloidally from the center to the outer edge of the plasma. Central current drive experiments using two gyrotrons with 1.5 MW of injected power drove about 0.17 MA. Results obtained using the DIII–D ECH systems will be reported.

## 1. INTRODUCTION

Electron cyclotron resonance heating (ECRH), has a multitude of applications beneficial to improved performance in tokamak plasmas. Tokamak plasma parameters can be enhanced by controlling the current density profile, leading to a high fraction of pressure produced bootstrap current (~80%), making non-inductive steady-state operation practical; by producing and extending an internal transport barrier to larger plasma radius, thus reducing the overall heat transport; and by suppressing performance robbing plasma-instabilities by local application of heat and current drive in the zones where instabilities are known to originate.

Since present day research devices and more importantly future reactor-like devices need multi-megawatt electron cyclotron heating (ECH) systems, it has been a long time goal of microwave tube manufacturers to develop a 100+ GHz tube that can operate at 1 MW, continuously, with a reasonably high efficiency. It appears that the internal mode-converter gyrotron with a CVD diamond window meets this objective. A gyrotron [1,2] is a microwave production tube that uses a hollow high velocity (70-100 keV) electron beam to excite a high Q cavity to resonate at the electron cyclotron frequency. To minimize the wall losses in the cavity, the cavity is designed to be highly over-moded but with sufficient separation between competing modes such that only the desired mode is excited by the electron beam. For the 1 MW, 110 GHz, CPI gyrotrons used on DIII–D, the cavity mode is $TEM_{22,6,1}$. The rf energy is extracted from the cavity and formed into a Gaussian beam by a Vlasov converter, as modified by Denisov [3], and a series of mirrors, which forms and directs the rf beam to exit the tube

* Communication and Power Industries, Palo Alto, CA, USA

through a low loss output window, which is located at or near the Gaussian waist. Thermal stresses developed in the output window have been the major technical roadblock to achieving a reliable 1 MW, cw, gyrotron. Sapphire and boron nitride have been successfully used in MW class gyrotrons with pulse length as high as 2 s. But it has only been with the development of low loss large CVD diamond disks that true 1MW, cw, gyrotrons have become available. Although CVD diamond material has been available for several years [4] there has been a difficult learning process in its application, which will be discussed below.

To transport the rf energy from the gyrotron to the tokamak, the DIII–D system uses an evacuated low-loss corrugated transmission line, up to 100 m in length with up to 14 $90^0$ mitre bends. The transmission efficiency of this system is about 80%. The transmission lines also incorporates customized diagnostic devices that are used to characterize the rf beam. These will be described in more detail in the following sections. Finally the plans for future enhancements to the DIII–D ECH system will be presented.

## 2. ECH SYSTEM & HARDWARE DEVELOPMENT

### Overview

The 110 GHz ECH system for the DIII–D tokamak consists of six assemblies (see Fig. 1). Each assembly consists of a gyrotron, a gyrotron superconducting magnet, a gyrotron/magnet supporting tank, a low loss transmission line, a launcher and associated controls. Three of the gyrotrons were manufactured by GYCOM* and have a nominal output of 800 kW 2 s, with the pulse length limit resulting from the peak temperature allowed on the boron nitride output window. The three long pulse gyrotrons are manufactured by CPI and have a nominal rating of 1 MW, 10 s. All sub-elements of these gyrotrons are expected to be in thermal equilibrium at 10 s, therefore a cw rating is possible for these units.

### Long Pulse Gyrotron

The three long pulse 110 GHz gyrotrons used in the DIII–D ECH system are an internal-mode-converter design (shown in Fig. 2) with a Gaussian output rf beam. Each gyrotron has a hollow annular electron beam produced by a magnetron injection type electron gun with a single anode (diode), which can operate up to 45 A. The hollow electron beam is compressed by the 44 kG field from the gyrotron super-conducting magnet, with the field maximum designed to occur at the center of the gyrotron cavity. At this location the beam diameter (~1 cm) and thickness (~1 mm) is adjusted such that only the $TEM_{22,6,1}$ cavity eigenmode is excited. The beam thickness is critical to pure mode operation since the over-moded cavity has a large number of modes spaced closely together. If any of the nearby modes are excited, they can rob power from the desired mode.

The rf power generated in the cavity has a complex structure that does not lend itself to low loss propagation. To achieve the desired low loss propagation, the rf wave must be formed into a Gaussian-like rf beam. The first step of this process is to make small perturbations in the launcher tube that bunch the rf energy together as the wave bounces along the spiral path as it exits the launcher. Since the cavity and launcher are deep inside the magnet bore, a series of relay mirrors is used to direct the rf beam out of the gyrotron. These mirrors can also be used to make final correction to the phase and profile of the beam such that at the output window, the beam has good Gaussian qualities. The use of mirrors also allows the rf beam to be decoupled from the electron beam with the rf exiting out the side of the gyrotron while the spent electron beam is deposited on a water cooled collector mounted above the output mirror/window beam is

* Gycom, 46 Ulyanov St., Nizhny Novgorod, Russia

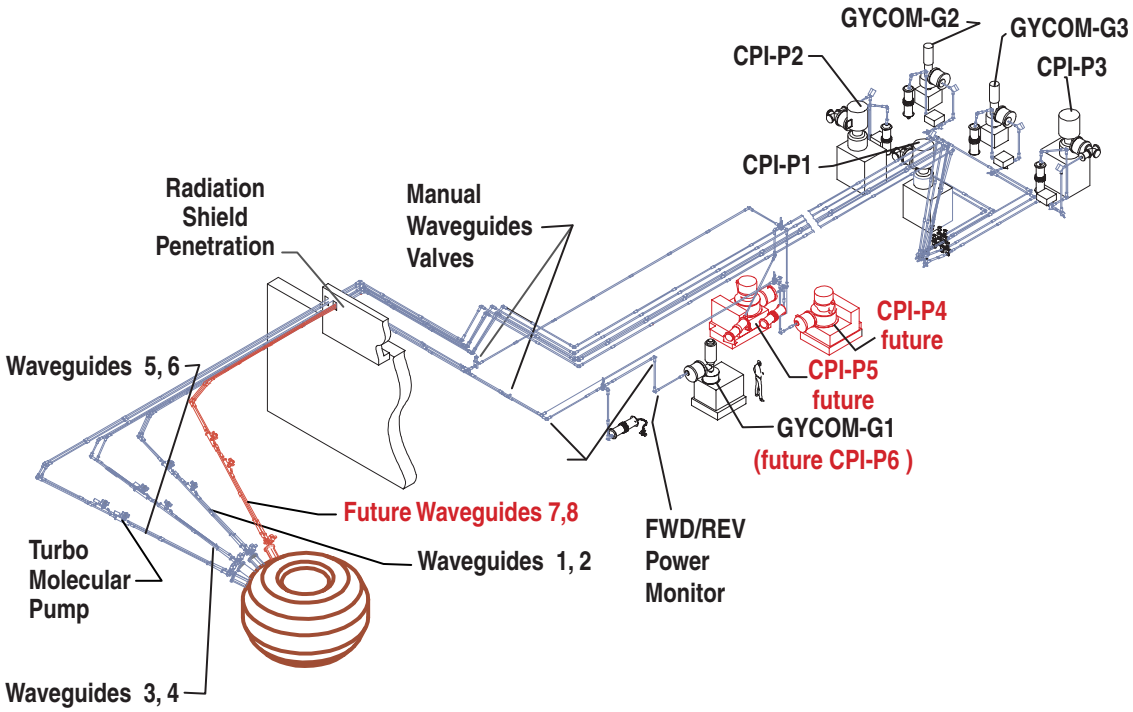


Fig. 1. Layout of the DIII–D ECH system including the future transmission lines and gyrotrons as well as key transmision line components.

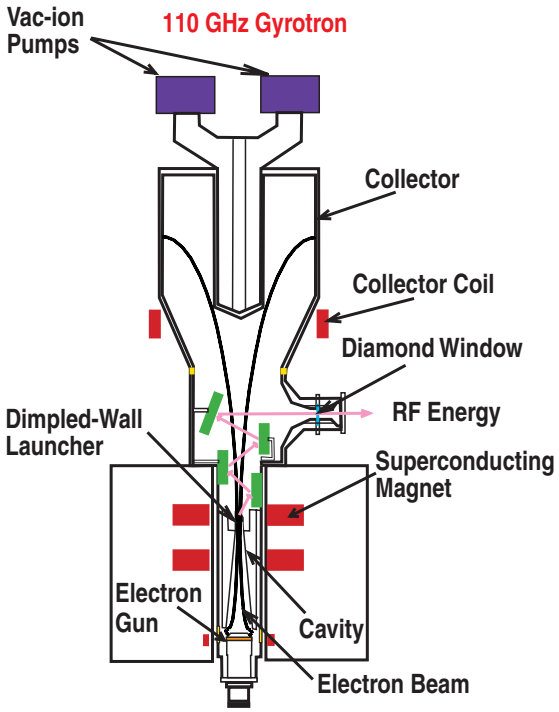


Fig. 2. Schematic diagram of 110 GHz, 1 MW gyrotron with CVD diamond output window.

deposited on a water cooled collector mounted above the output mirror/window assemly. All the sub-elements that may intercept either the rf beam or electrons are made from copper and are water cooled with a cw rating at full power. The gyrotron is vacuum pumped by dual 20 l/s vac-ion pumps, and the collector is electrically isolated from the gyrotron body by a ceramic break. The isolation allows for a convenient method of centering the beam inside the cavity by monitoring the low level body current signal.

## CVD Diamond Window

The advent of large size Chemical Vapor Deposition (CVD) synthetic diamond windows, with low rf loss, has ushered in the feasibility of truly high power cw gyrotrons. Previous gyrotron output window material had either relatively high loss, 4% for boron nitride, or poor thermal conductivity (sapphire), that limited the pulse length at 1 MW to a few seconds at best. These windows also required spreading the rf beam in a non-Gaussian profile, which needed to be converted back to Gaussian external to the

gyrotron, resulting in at minimum a loss of 10% of the rf power. CVD diamond also has the beneficial characteristic of a high thermal conductivity of 6.5 kW/m$^2$°K, about four times that of copper, which allows simple edge cooling to extract all the energy absorbed (~0.2%) as the rf beam passes through.

The application of CVD diamond as an output window did not come without several technical challenges. Diamond by its nature has a very low thermal expansion co-efficient, much lower then any of the metals one would propose using in making a vacuum seal. Thus the first vacuum seals attempted relied on a low temperature diffusion bond using pure aluminum. The diffusion bond allowed the seal processing temperature to be low, and the softness of the aluminum reduced any stresses caused by differential thermal expansion. The use of aluminum had three significant problems in actual use. First the aluminum was subject to aggressive water corrosion, which even with corrosion inhibitors in the water, led to several vacuum failures, two at General Atomics and several worldwide. Second, the tube could not be processed after assembly at the normal 500$^+$°C, but had to be kept below 450°C, otherwise the aluminum bond would soften leading to a seal failure. Third, some windows cracked at low power levels owing to a lossy hydrogen film, believed to be created on the surface of the window during the diffusion bonding process.

An anticipated solution to the above issues was the development of a AuCu high temperature braze between the diamond and a copper seal ring. It was shown that such a braze could be made to a 63.5 mm dia. 1.14 mm thick CVD disk, giving a 50 mm clear aperture for the rf beam. Two gyrotrons with this design were built for the DIII–D program, with the first unit passing a 600 kW, 10 s factory test before being delivered to the DIII–D program. However during the testing of the second gyrotron at CPI the window failed when a 20 mm crack developed from the center to the edge. The failure had the characteristics of a thermally induced stress crack, which was unexpected since even at 1MW the thermal stress level should have been a factor of two lower than the expected 350 MPA yield stress for CVD diamond.

Following the failure an investigation was mounted to determine the root cause of the failure and to validate the braze process before any more gyrotrons were to be assembled. The failed window along with the windows that had been brazed but not installed, as well as unbrazed window blanks were re-measured to determine if the loss tangent had changed. It should be noted that by this time the high losses caused by the hydrogen contamination of the aluminum bonded windows had become known. Loss tangent measurements indicated that the losses in AuCu brazed windows had increased during brazing, with the worst case being a factor of 8 higher than the blank disk of $\leq 1\times10^{-4}$. The power lost in the failed window assembly was consistent with a loss factor of $3.8\times10^{-4}$, and the window disk then would have a thermal stress level of 350 MPA at about 600 kW transmitted power.

In evaluating the cause of the enhanced loss factor, the window disks were measured for impurities using a 514 μm laser Raman scattering system. This investigation revealed a thin (≤1 μm) layer of graphite on the surface of the window but no bulk contamination. It was also shown that this graphite layer could be removed by grit blasting with 3 μm alumna powder as shown in Fig 3. The DIII–D program had one of the AuCu brazed window gyrotrons in service when this enhanced loss issue was discovered. In order to minimize the risk of failure, the gyrotron was initially limited to maximum operating conditions of 800 kW, 2s. Once the cause of the enhanced loss was identified to be a graphite film the window was grit blasted in-situ and then tested by pulsing the gyrotron and observing the window temperature with an IR camera. Before and after IR images of the window are shown in Fig.4.

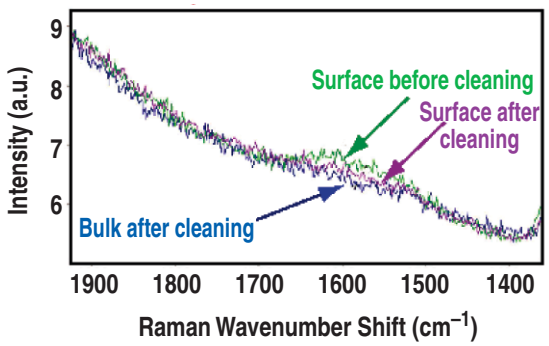


Fig. 3. In-situ Raman spectra of the CPI-P2 gyrotron CVD diamond window near the graphite wavenumber of ≈1600 cm$^{-1}$. Measurements of the surface before and after cleaning with 3 μm alumna powder, and a measurement of the bulk diamond is shown.

Following the cleaning, the gyrotron was able to run at close to 1 MW for 5 s without the window temperature exceeding 150$^{O}$C. Comparing the window temperature measurements to those calculated for 1 MW shows that the effective loss tangent is well below the required 1×10$^{-4}$, (see Fig. 5). Figure 6 shows that the window comes into thermal equilibrium in about 3 s.

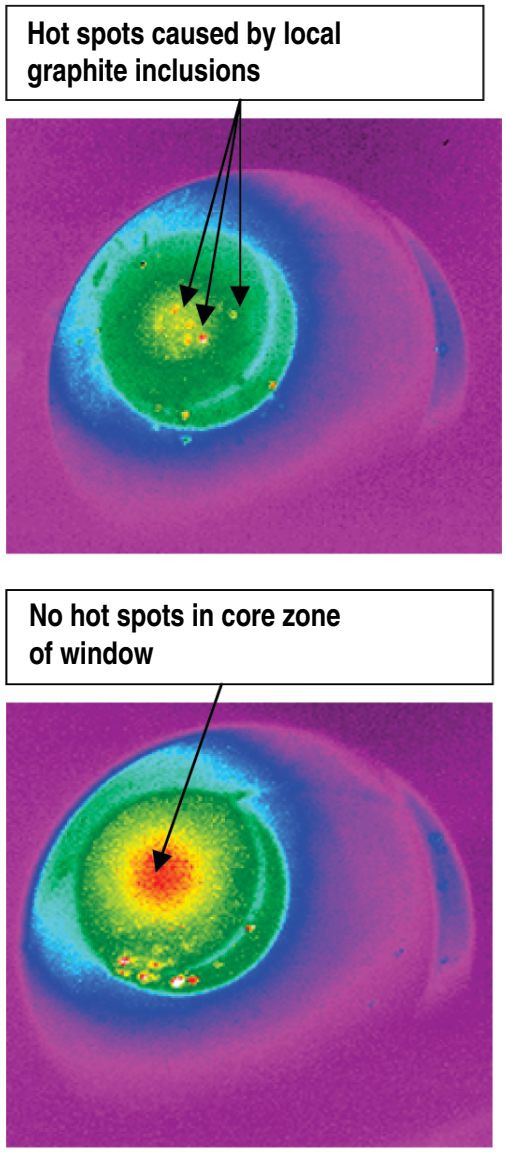


Fig. 4. IR images of the CVD diamond window before and after cleaning with 3 μm alumina grit. Note the removal of localized hot spots believed to be caused by local graphite inclusions. The hot spots at the bottom of the ''after'' image are thought to be the fluorescence of dust by low power rf, since there is no substantial power in the rf beam at this location.

## Transmission Line System

The transmission line system connects the gyrotron to the launcher on the DIII–D tokamak using evacuated corrugated waveguide with a 31.75 mm inside diameter. To couple the Gaussian rf beam exiting the gyrotron 52 mm diameter output window to the 31.75 mm waveguide only requires one mirror that is placed about one meter from the output window. The mirror is a simple focusing mirror cut using Gaussian optics criteria to match the beam at the entrance to the waveguide. Micrometer positioners on the mirror mounts allow for fine tuning the location of the beam waist at the wave guide entrance. An accuracy of less than 1 mm is required. The tee holding the mirror provides a convenient location for vacuum pumping for the evacuated waveguide and to have viewing ports for observing the gyrotron window during operation.

In order to tune and assess the performance of the gyrotron before injecting power into the tokamak, the rf power is directed into a dummy load placed as close to the gyrotron as practical. The redirection of the rf beam is performed by a waveguide switch that inserts a 45$^{O}$ mirror in the transmission line. It is important that any dummy load used to test high power

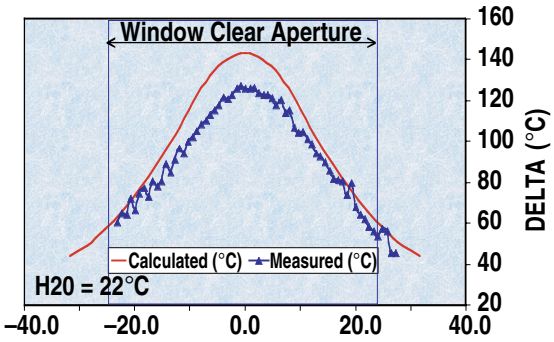


Fig. 5. Temperature profile measured and calculated for a 50 mm clear aperture CVD diamond gyrotron output window for a ≈ 1 MW, 5 s pulse. Cooling water 22°C.

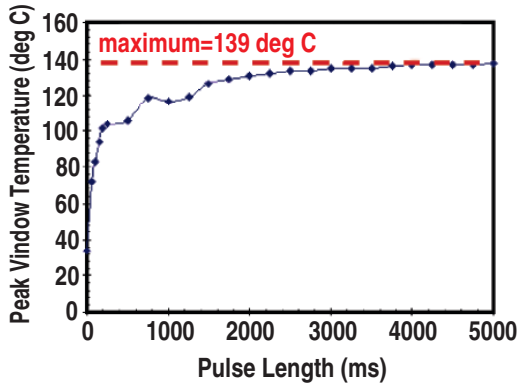


Fig. 6. Peak window temperature for a ≈ 1 MW, 5 s pulse. Cooling water temperature 22°C.

gyrotrons have a very low reflection coefficient, i.e., the load must look very black. The evacuated dummy load developed to handle the 1 MW, 10 s pulses with no reflections, was based on converting the low loss $HE_{11}$ rf beam, which has small to non-existent wall currents, to a TM mode with wall currents that dissipate their energy on a water cooled section of lossy wave guide. The final design uses a 2 m section of a specially machined Glidcop® copper waveguide with the interior corrugations plated with nickel to increase the losses. This load, shown in Fig 7, absorbs 800 kW cw, or 80% of the input power. The remainder of the power is absorbed in a normal open-tank dummy load made from Inconel.

The rf beam launched into the plasma comes from the outside of the tokamak (low field side) and is at the second harmonic of the electron cyclotron frequency (to increase the accessible density to about $7\times10^{19}/m^3$ before cutoff is reached). For optimum coupling of the rf beam at a desired location, extraordinary mode polarization (X-mode) is used. When the power is injected obliquely to drive current the polarization must be elliptical to excite the X-mode. The ellipticity and angle

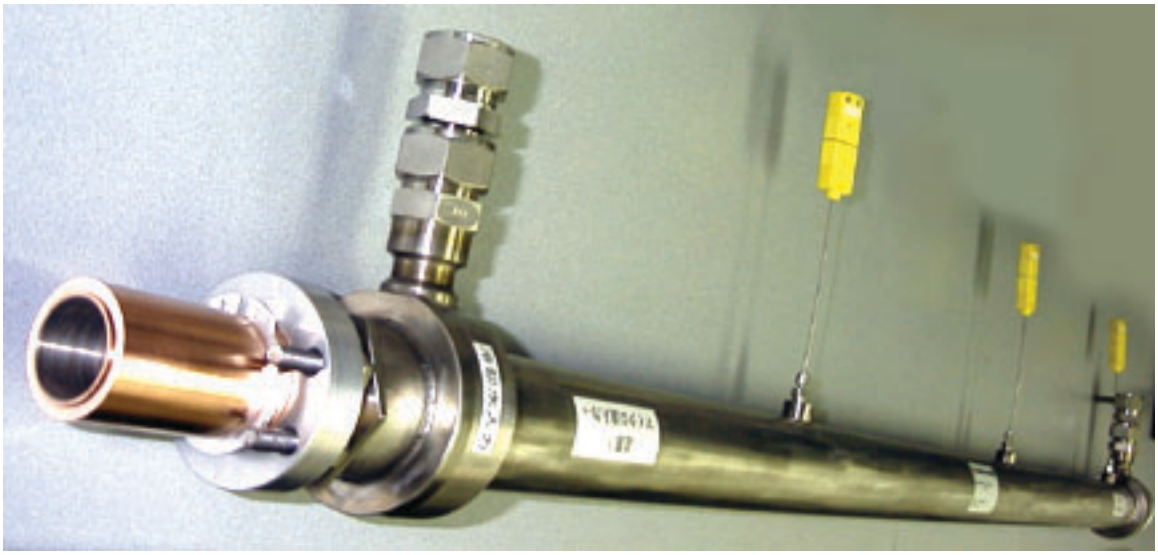

Fig. 7. Compact dummy load made from a lossy copper waveguide section inserted into a water jacket. A 2 m load can eremove 800 kW cw, with little or no reflection.

of polarization is controlled by a set of grooved mirrors located in the transmission line. At two mitre bends the normal flat mirrors are replaced with rotatable water-cooled grooved mirrors, the first mirror has a groove depth of $\lambda/2$ which rotates the plane of the linearly polarized wave, and the second mirror has a groove depth of $\lambda/4$ which controls the ellipticity [5]. The mirror rotation angle is determined using a computer model that takes into account the specifics of the transmission line geometry, (each mitre bend rotates the polarization angle), the plasma current, the base magnetic field, the launch mirror angles and the plasma density. Measurements of the linear polarization at the last mitre bend before the launcher showed greater than 95% of the power was in the desired polarization for several combinations of polarization angles and polarizer mirror settings.

To facilitate all the experiments that require the use of ECH, the launchers, located on the outer upper ports of the DIII–D vacuum vessel, must have the ability to scan the rf beam both poloidally and toroidally in order to locate the beam on- and off-axis; and to support both co- and counter-current drive. An additional challenge is that two launchers and their mirror steering mechanisms must reside inside a port box approximately 300×400 mm , which is 1 m in length.

Each launcher has a fixed focussing mirror and a flat steering mirror. Owing to concerns over water leaks these mirrors are not water-cooled, but depend on radiation cooling between shots to keep the mirrors within operating temperatures. Two designs to achieve the 10s pulse length capability are being evaluated. One design uses a solid Glidcop copper mirror which has been tailored to have a thick slug of copper on the back [6] at the center, where the power loading is highest, in order to wick away the deposited energy, keeping the peak temperature within bounds. The back surface of the mirror is grooved and blackened to raise its emissivity to over 90% to enhance radiation cooling. The second design, features a butcher block copper/stainless steel laminated structure [7] where the copper acts as a thermal heat sink and the stainless provides strength and reduces the eddy currents which caused unwanted torque on the steering mechanism. This design also uses radiation from the backside to cool the mirror between shots. Presently there are three dual launchers on DIII–D and there is one more port with the dimensions for a possible fourth launcher. Figure 8 shows a picture of the newest dual launcher, which was built by Princeton Plasma Physics Laboratory (PPPL) and incorporates the butcher block mirror design.

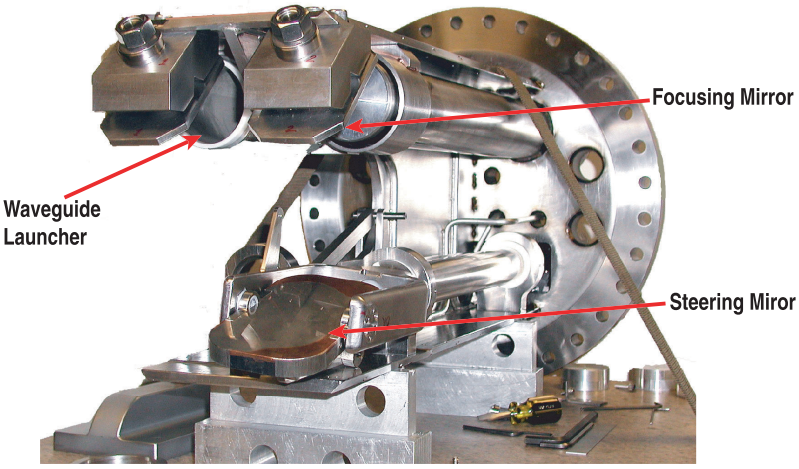


Fig. 8. Photo of a dual steerable ECH launcher designed and built by the Princeton Plasma Physics Laboratory. Each launcher incorporates a fixed focusing mirror and a flat steering mirror. The steering mirror can rotate over a range of $\pm 20^{0}$ poloidally and toroidally.

## 3. EXPERIMENTAL RESULTS

### Current Drive

Plasma performance can be enhanced by modification of the pressure or current density profile j(r). ECH with its precisely localized heat and current drive capabilities is an excellent tool to support the exploration of advanced tokamak physics activities [8]. ECH current drive efficiency is proportional to the electron temperature, thus it is more effective at the center of the plasma where the temperature peaks. There was a concern that the efficiency of the off-axis current plasma where the temperature peaks. There was a concern that the efficiency of the off-axis current drive would be unacceptably low at the edge of the plasma where it was needed for AT plasma and stability control. The decreased efficiency is not only caused by a lower plasma temperature but also by trapping effects which push electrons into trapped orbits in which they cannot contribute to current drive. However, initial off-axis experiments at the megawatt level and now theoretical modeling do not show the dramatic drop of in current drive as shown in the low β case in Fig. 9. The key to this phenomenon is that as the local electron beta ($\beta_e$) is increased the electrons are moved away from the trapping orbits and more electrons participate in driving current. Electron cyclotron driven currents of 120 kA have been measured on DIII–D with excellent agreement with the Fokker-Planck Theory.

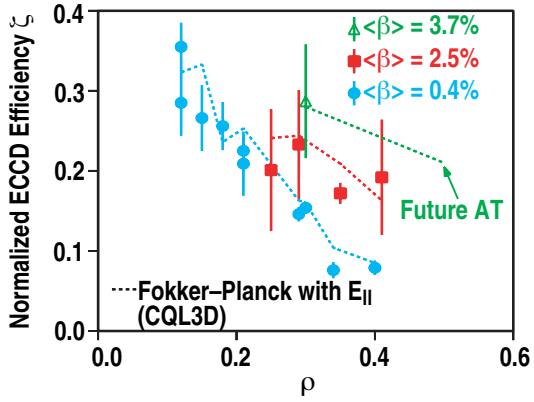


Fig. 9. Experimental ECCD efficiency as a function of the normalized radius of deposition for an L-mode plasma with <β>=0.4% (circles), an H-mode plasma with <β>=2.5% (squares), and an advanced tokamak with <β>=3.7% (triangle). The theoretical ECCD efficiency is also shown (dashed lines).

### NTM Stabilization

The Neoclassical Tearing Mode (NTM) is generated when the boot strap current driven by the local electron pressure gradient can not be supported. The electron density depression usually occurs at low order rational surfaces (e.g., q = 3/2, 2/1), with the 3/2 mode being the most dominant [9]. Because the absorption length of the rf beam is close to the thickness of the magnetic island created by the NTM, and the physical size of the beam is small compared to the island size, ECCD can be used to shrink or eliminate the magnetic island of the tearing mode. Experiments on DIII–D had demonstrated a complete suppression of the 3/2 NTM mode, which resulted in a plasma performance exceeding the threshold level, which triggers

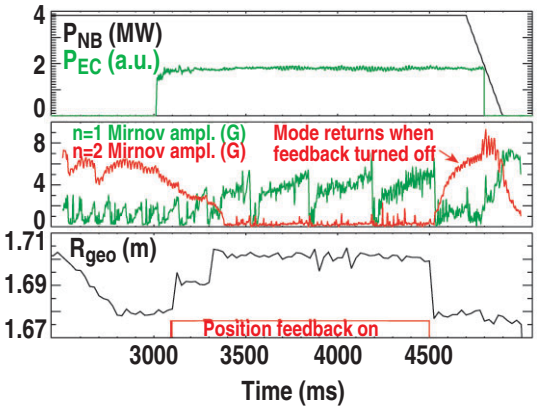


Fig. 10. Approximately 2.3 MW of ECCD is used to suppress a m/n=3/2 NTM in discharge #107396 after which neutral beam power is raised to increase beta. $\beta_N$ is increased by 55%.

the NTM mode, as long as the ECH power was on. This result is clearly shown in Fig. 10. lt is clearly shown in Fig. 10. NTM suppression is very sensitive to the placement of the rf beam, a radial shift of the 8 cm diameter beam by as little as 2 cm almost cancels the suppression effect [10].

## Transport

The small size of the rf beam as well as the ability to modulate the power has made ECH an efficient tool to measure the local electron energy transport. By tracking the diffusion of the energy deposited by a short burst of rf power at the resonance zone, the local electron energy transport coefficient can be directly measured. By injecting a train of pulses very sensitive Fourier Transform methods can be used. Figure 11 shows a typical use of modulated ECH where the response of several channels of the electron cyclotron emission (ECH) diagnostic, at a number of spatial points on either side of the deposition zone, allows the tracking of the magnitude and phase delay of the injected power. Fitting the time response at each radius allows for the calculation of the spatial variation in the energy confinement time and the transport coefficients.

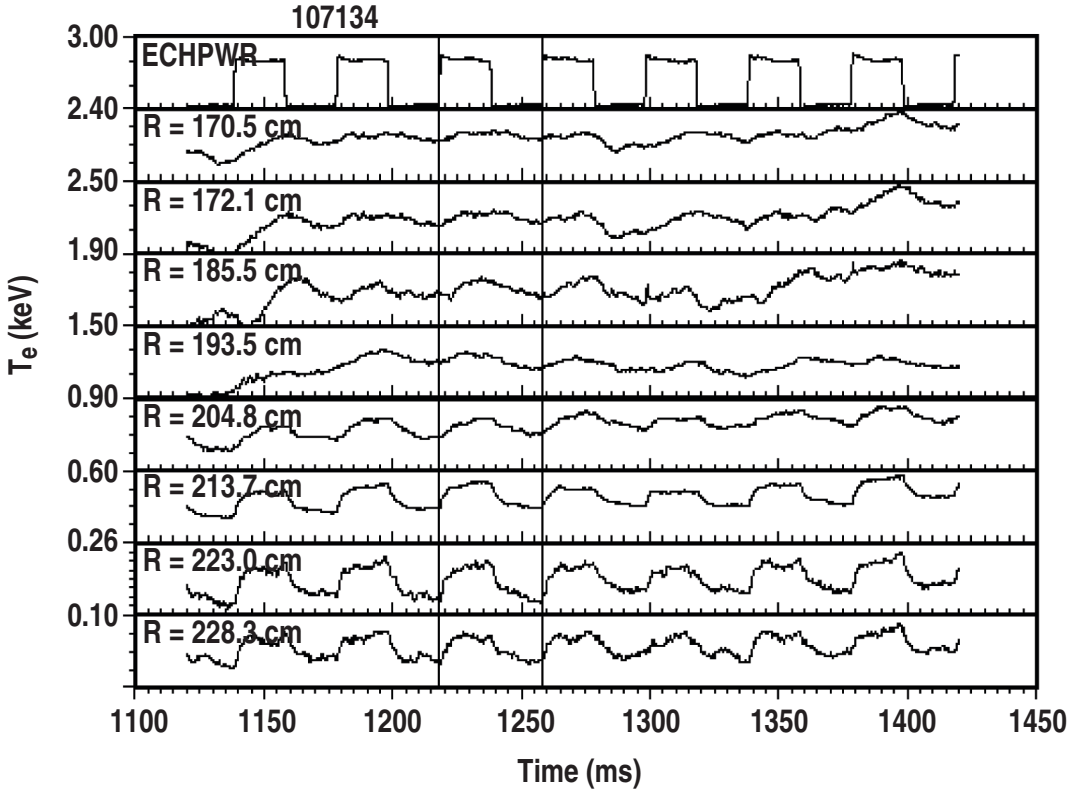


Fig. 11. The rf power, about 2.0 MW modulated at 25 Hz, was deposited close to the plasma edge at R~220 cm. The effect on the electron temperature can be seen throughout the plasma with a slight phase shift for locations far from the deposition location. The shape of the ehating effect gives directly the local incremental confinement time. Perpendicular rf injection was used to localize the deposition.

## Electron Thermal Barrier

Discharges with internal transport barriers (ITB), or regions of reduced transport, in the ion thermal, particle and/or angular momentum transport channels have been developed which exhibit high fusion performance in many tokamaks. Recently, several tokamaks have

demonstrated barrier formation in the electron channel in the presence of intense, localized, direct electron heating [11]. Such a regime has now been demonstrated in discharges heated primarily by electron cyclotron heating (ECH) in the DIII–D tokamak.

The e-ITB appears promptly in the early phase of discharges operated at low density ($n_e<1\times10^{19}$ $m^{-3}$), when ECH is applied 0.1 s after the beginning of the current ramp (Fig. 12). The discharge shown is heated by the output of a single gyrotron, which provides 0.5 MW of heating power to the electron component of the plasma. Although the ECH is phased to generate electron cyclotron current drive (ECCD) in the direction opposite to the main plasma current (counter-ECCD), nearly identical results have been achieved in DIII–D with both co-ECCD and pure heating (waves launched radially into the plasma so as to drive no net current).

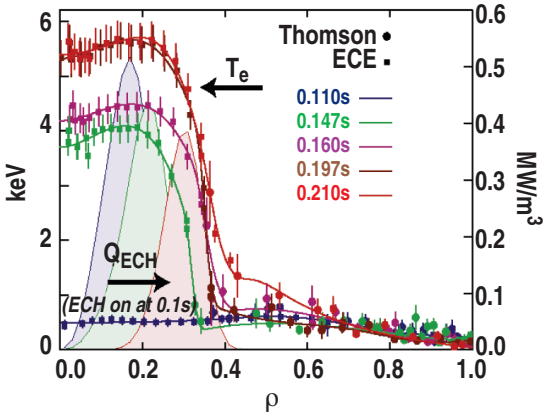


Fig. 12. Electron transport barrier forms immediately upon application of ECH of 0.5 MW. Barrier lies just outside heating location.

The electron temperature profile responds almost immediately to the onset of ECH. A steep temperature gradient, which can exceed 150 keV/m in an approximately 3 cm wide region, forms near the heating location. Central temperatures reach 4 keV in the first 37 ms of the ECH pulse, and 6 keV in less than 100 ms. This barrier appears to expand ahead of the heating location as that location is shifted outward due to increasing density and by the Doppler shift as the temperature increases. A small increase is seen in the ion temperature as well, but the ions remain relatively cold, with $T_e/T_i\approx10$ in the core.

## 4. FUTURE PLANS

The DIII–D program is planning to advance to six 10 s gyrotron systems using the existing designs. Experiments to date have indicated that increased power and pulse length will be required fully to exploit the advantages of ECH/ECCD for tokamak operation. The DIII–D tokamak has four ports available that can support the dual launcher assemblies, this will allow the power to be almost tripled for pulse lengths of 5–10 s provided all eight gyrotrons can be accommodated in these ports, particularly if higher unit power becomes available.

## Acknowledgements

This is a report of work supported by U.S. Department of Energy under Contract Nos. DE-AC03-99ER54463 and DE-AC02-76CH03073. The authors wish to thank Dr. R. Heidinger and his staff from the Institute for Material Science, Karlsruhe, Germany, for many measurements of the loss tangent of the diamond windows; and also Dr. V. Erck mann, from the Max-Planck-Institute for Plasma Physics, Greifswald, Germany, for loaning the DIII–D program two diamond windows to expedite the repair of the gyrotrons.

## References

[1] M.V. Agapova *et.al.*, Proc. 20th Int. Conf. on Infrared and Millimeter Waves, Ed. R. Temkin, Coca Beach, Florida, p. 205 (1995).

[2] K. Felch *et al.*, Proc 22st Int. Conf. on Infrared and Millimeter Waves, Colchester, England, 1998, to be published.
[3] G.G. Denisov, A.N. Kuftin, V.I. Malygin, N.P. Venedictov, and V.E. Zapevalov, Int J. Electronics **72**, 1079 (1992).
[4] K. Takahashi, K Sakamoto, A. Kasugai, T. Imai, J.R. Brandon, and R.S. Sussmann, Rev. Sci. Instrum. **71**, 4139 (2000).
[5] J.L. Doane, Int. J. Infrared and Millimeter Waves **14**, 363 (1992).
[6] C.B. Baxi, M.E. Friend, E.E. Reis, R. Prater, R.W. Callis, and R.A. Legg, to be published in the 19th Symposium on Fusion Engineering, Atlantic City, N.J., 2002.
[7] R. Ellis *et al.*, to be published in the 19th Symposium on Fusion Engineering, Atlantic City, N.J., 2002.
[8] C.C. Petty *et al.*, Proc. 14th Topical Conference on Radio Frequency Power in Plasmas, Oxnard, CA ( 2001), p.275.
[9] B. Lloyd, Proc. 14th Topical Conference on Radio Frequency Power in Plasmas, Oxnard, CA ( 2001). P. 33.
[10] T.C. Luce, R.J. LaHaye, D.A. Humphreys, C.C. Petty, and R. Prater, 14th Topical Conference on Radio Frequency Power in Plasmas, Oxnard, CA ( 2001), p. 306.
[11] C.M. Greenfield *et al.*, submitted for publication in Phys. Rev. Lett.